Surface three-dimensional velocity map imaging: A new technique for the study of photodesorption dynamics

Yuanyuan Ji, Sven P. K. Koehler, Daniel J. Auerbach, and Alec M. Wodtke

---

Articles you may be interested in

Surface three-dimensional velocity map imaging: A new technique for the study of photodesorption dynamics

Yuanyuan Ji
Department of Chemistry and Biochemistry, University of California, Santa Barbara, California 93106

Sven P. K. Koehler
Department of Chemistry and Biochemistry, University of California, Santa Barbara, California 93106
and School of Chemistry, University of Manchester, Manchester M13 9PL, United Kingdom

Daniel J. Auerbach[a]
Department of Chemistry and Biochemistry, University of California, Santa Barbara, California 93106
and GRT Inc., 861 Ward Dr., Santa Barbara, California 93111

Alec M. Wodtke
Department of Chemistry and Biochemistry, University of California, Santa Barbara, California 93106

The authors describe the application of a combination of velocity map imaging and time-of-flight (TOF) techniques to obtain three-dimensional velocity distributions for surface photodesorption. They have established a systematic alignment procedure to achieve correct and reproducible experimental conditions. It includes four steps: (1) optimization of the velocity map imaging ion optics' voltages to achieve optimum velocity map imaging conditions; (2) alignment of the surface normal with the symmetry axis (ion flight axis) of the ion optics; (3) determination of TOF distance between the surface and the ionizing laser beam; (4) alignment of the position of the ionizing laser beam with respect to the ion optics. They applied this set of alignment procedures and then measured $Br(^2P_{3/2})$ (Br) and $Br(^2P_{1/2})$ (Br*) atoms photodesorbing from a single crystal of KBr after exposure to 193 nm light. They analyzed the velocity flux and energy flux distributions for motion normal to the surface. The Br* normal energy distribution shows two clearly resolved peaks at approximately 0.017 and 0.39 eV, respectively. The former is slightly faster than expected for thermal desorption at the surface temperature and the latter is hyperthermal. The Br normal energy distribution shows a single broad peak that is likely composed of two hyperthermal components. The capability that surface three-dimensional velocity map imaging provides for measuring state-specific velocity distributions in all three dimensions separately and simultaneously for the products of surface photodesorption or surface reactions holds great promise to contribute to our understanding of these processes. © *2010 American Vacuum Society.* [DOI: 10.1116/1.3327929]

I. INTRODUCTION

Developing a molecular level understanding of how chemical processes occur in terms of the potential energy surfaces governing the processes and the motion of the participating molecules on these surfaces is a basic goal in the field of chemical dynamics. One of the most important tools used in pursuit of this goal is the measurement of the angular and velocity distributions of the product molecules.[1–3] Measurements of molecular speed are often made using the time-of-flight (TOF) technique,[4] which requires a detector that is sensitive to a narrow angular range. By moving the detector from one angle to another, it is possible to measure the TOF intensity as a function of angle, which can be used to derive a three-dimensional velocity distribution. This procedure is effective but can be laborious and time consuming.

In a landmark 1987 paper, Chandler and Houston[5] showed how measurement of velocity distributions could be streamlined by the use of ion imaging techniques to obtain two-dimensional velocity distributions in a single image. They used lasers to selectively ionize the product molecules, accelerated the ions, and let them fly to an imaging detector. The point at which the molecules hit the detector was related to their velocity perpendicular to the accelerating field and thus the image could yield information about the two-dimensional velocity distribution of the process under study. Because the velocity distribution along the accelerating field was crushed essentially to a single velocity in the direction parallel to the accelerating field, this technique is sometimes referred to as velocity crush ion imaging.

The velocity resolution of ion imaging was greatly improved with the development of velocity map imaging (VMI) by Eppink and Parker.[6] VMI uses an electrostatic lens to map the perpendicular velocity to a point on the imaging detector. Unlike velocity crush imaging, in VMI the position of the particle when it is ionized does not influence the point at which it strikes the detector; only the two components of velocity in the plane perpendicular to the accelerating field are important. The insensitivity to initial position is achieved by having the plane of ionization effectively at the focal plane of the ion optical system. The elimination of a spatial

---

[a]Electronic mail: auerbach@mailaps.org

influence on the point of impact on the detector greatly improves the resolution and capabilities of velocity imaging techniques.

Both velocity crush imaging and the more recent VMI have been widely used in the study of gas phase chemical processes,[7] but their use for processes occurring at surfaces has been much more limited. Only a handful of applications of velocity crush imaging have been reported for surface processes.[8–12] Recently, we demonstrated the use of VMI to measure three-dimensional velocity distributions of $Br(^2P_{3/2})$ and $Br(^2P_{1/2})$ atoms (which we hereafter refer to as Br and Br*) resulting from photodesorption from the surface of a KBr crystal.[13] We chose this system as a test case for the technique since it had been previously studied by other methods.[14,15] By using a combination of TOF and VMI techniques, we were able to obtain three-dimensional velocity map images of desorbing Br and Br*, that is the desorption probability, P, as a function of three Cartesian components (v_x, v_y, and v_z) of the velocity vector, $\vec{v}$. Our measured velocity and angular distributions are qualitatively similar to the previous work on this system but revealed new features of the desorption dynamics. Most notably, we observed evidence for multiple hyperthermal desorption channels.

During the course of this work we encountered problems with the reproducibility of the velocity images. The difficulties were related mainly to difficulties in reproducible setting the alignment of the apparatus. Furthermore, in analyzing the data, we became aware that the size of the ionization region in the direction along the ionization laser beam might be distorting our velocity images.

Here, we present results from an improved version of the three-dimensional surface VMI technique and we describe in detail a systematic method for alignment of the laser beam and surface relative to the VMI ion optics. The alignment is accomplished using the properties of the ion optics and the measured signal (TOF, spatial, and velocity map images) rather than by means of fixed mechanical fiducial points. We also improved the detection geometry by using a tighter focus on the ionization laser to more nearly approach a true "sheet-point" geometry. We present results on the TOF, velocity, and energy distributions in the direction normal to the surface and compare these results to previous work.

II. APPARATUS

The apparatus and surface preparation techniques have been described previously.[13] For completeness, we give a brief description here with emphasis on changes from the previous setup and the features that are important for this work.

The basic principle of the experiment is to use a pulsed laser to stimulate desorption from the surface, a second laser to ionize the desorbing atoms after a defined flight time between the surface and the ionization volume, and VMI optics to measure the velocity components of the resulting ions in the direction parallel to the surface (v_x and v_y). By adjusting the time delay between the two lasers, we can select desorbing atoms moving with a specific velocity component normal
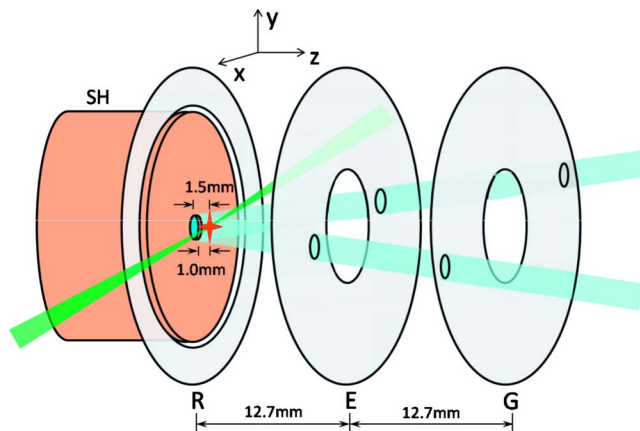

FIG. 1. (Color online) Schematic of the electrostatic lens assembly of the surface velocity map imaging setup. The KBr surface is mounted on the sample holder (SH), shown as the cylindrical object. The illuminated area that is indicated as the dark shaded area in the center of the repeller plate is 6 mm in diameter. The focal point of the REMPI laser is 1.5 mm away from the KBr surface and 1.0 mm away from the repeller plate (R). Two sets of small holes symmetrically located in the extractor (E) and ground plate (G) are used to allow the desorption laser beam to strike the surface. R-E and E-G spacing is 12.7 mm and the flight tube length is 1050 mm.

to the surface (v_z). For subsequent discussion we define the principle directions used in the experiment: z is the direction perpendicular to the surface, x is parallel to the surface and along the propagation direction of the resonance enhanced multiphoton ionization (REMPI) laser, and y is parallel to the surface and perpendicular to x.

As shown in Fig. 1, we use a standard three electrode VMI ion optics setup with a repeller, extractor, and ground plates.[6,16,17] The KBr crystal is mounted on an UHV manipulator with heating and liquid nitrogen cooling. A thin copper plate (0.5 mm) is mounted on top of the surface with a 6 mm diameter hole in the center which allows for excitation laser to get access to the surface. The sample holder in turn fits into a circular centered hole in the repeller plate. It is important that the surface of the sample holder be parallel and coplanar with the repeller so as not to distort the electric fields of the VMI ion optics. It was not sufficient to mechanically align the sample mount to the repeller plate before pumping the system down. In Sec. III we will describe how this alignment can be accomplished under vacuum using the properties of the velocity map images.

Desorption of Br and Br* is stimulated by laser irradiation of the KBr surface at 193 nm with the output of an ArF excimer laser at an angle of 45° relative to the surface normal. The laser beam fills the 6 mm diameter aperture in front of the crystal. Using fine wire mesh, we attenuated the pulse energy to 30 μJ to avoid surface damage.

Detection of Br and Br* is done via REMPI at ~234 nm. We chose the $6p\ ^4P^\circ_{3/2} \leftarrow \leftarrow ^2P^\circ_{3/2}$ (Br) and $6p\ ^2S_{1/2} \leftarrow \leftarrow ^2P^\circ_{1/2}$ (Br*) two-photon resonances at 233.6 and 235.2 nm, respectively. The REMPI laser is focused by a 20 cm focal length lens, rather than the 38 cm lens used in our previous work.[13] We chose a shorter focal length lens to reduce the two-photon Rayleigh length; that is, the length of the detec-
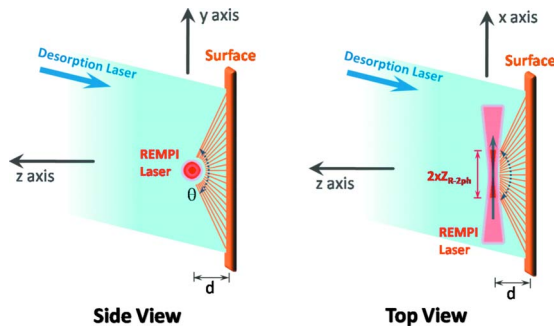
FIG. 2. (Color online) Schematic view of the excitation and detection geometry. Side and top views of the excitation and detection "sheet-point" geometry are shown. The KBr surface is drawn as the thin rectangle on right. The light shaded beam directed onto the surface represents the desorption-laser beam. The REMPI laser beam travels along the *x*-axis as shown in the top view on the right, with an ionization region depicted darker in the center of the beam. In the side view, the REMPI laser beam is viewed perpendicular to *y-z* plane. An angle Θ indicates the range over which those particles desorbed from the KBr surface would be ionized by REMPI laser. The time-of-flight distance, *d*, is 1.5 mm.

tion volume along the REMPI laser direction from the beam waist to the point where we have 50% ionization efficiency,

$$Z_{R-2ph} = \sqrt{\sqrt{2}-1}\,\frac{\pi\omega_0^2}{\lambda} = 4\sqrt{\sqrt{2}-1}\,\frac{f^2\lambda}{d^2\pi}, \qquad (1)$$

where f is the focal length of the lens, λ is the wavelength, and d is the diameter of the laser beam before focusing. For a beam that is 5 mm diameter before focusing, the two-photon Rayleigh length is 1.1 mm for a 38 cm lens and 0.31 mm for a 20 cm lens. The corresponding beam waists, ω_0, are 11 and 6 μm, respectively.

Figure 2 is a schematic diagram of the excitation and detection geometry. We use a broad excitation region (6 mm diameter) and a much smaller detection region (approximately 0.6 mm long by 12 μm in diameter). We refer to this geometry as the "sheet-point" detection geometry, similar to that used in sliced VMI.[18] It might seem more intuitive to use a setup with a small excitation region and a much larger REMPI ionization region ("point-sheet" geometry); however, this approach has serious disadvantages including increased surface damage from the focused desorption laser and decreased ionization efficiency in the REMPI detection. By making the ionization region large enough, this point-sheet geometry does however ensure that atoms leaving the desorption spot over a wide range of angles can all be detected. This is also possible with a "sheet-point" geometry. In this case, atoms leaving a given region of the surface are only detected over the small range of desorption directions that intercept the small detection volume. However, sensitivity to a broad range of desorption angles is obtained by building up contributions from a broad region on the surface. The "sheet-point" geometry has several important practical advantages.

(1) The use of a broad excitation region results in a lower power density at the surface and thus less surface damage for a given desorption flux,

(2) The use of a small spot for detection results in good TOF resolution. Note that although the REMPI laser to surface distance is only 1.5 mm, our TOF resolution is determined by the ratio of this distance to the average beam diameter. Using equations for Gaussian beam optics we estimate the resolution is $\gtrsim$150. Similar resolution can also be achieved with a "point-sheet" geometry if the REMPI laser is focused to the same beam waist using a cylindrical lens.

(3) The detection sensitivity is improved due to the higher power density in the detection volume obtained using a spherical focusing lens in comparison to a cylindrical lens.

(4) The use of a small ionization region insures that ions in the VMI ion optics are formed near the symmetry axis of the ion optics. This minimizes the effects of aberrations in the ion optics.

III. CALIBRATION AND ALIGNMENT METHODS

Proper alignment of the surface, excitation laser, REMPI laser, and VMI ion optics is essential in obtaining reliable and reproducible results from surface three-dimensional VMI. Some aspects of the alignment are easily controlled by mechanical means. For example, due to the relatively large size of the desorption region, alignment of the desorption laser beam relative to the crystal is not very critical and is controlled by passing the laser beam through holes in the extractor and ground plates (see Fig. 1). Other aspects of the alignment are more critical. These include properly setting the following: (1) the ratio between voltages on the repeller and extractor required for optimum VMI conditions; (2) the parallelism of the surface of the crystal holder and the repeller; (3) the distance of the REMPI laser from the surface, z_{REMPI}, which is particularly critical since it determines the calibration of measurements of the z component of the velocity; (4) the position of the REMPI laser focus in the x and y directions relative to the VMI ion optics. We have developed a series of methods to do the alignment of each of these aspects without the need for mechanical fiducial points. Rather than using fiducial points, the methods use measurements of the ion signal as the alignment is adjusted exploiting the properties of the VMI optics. We now describe each of these methods briefly in turn.

A. Voltages for velocity map imaging and VMI velocity calibration

The proper ratio of voltages on the repeller and extractor ($R_{VMI} = V_E/V_R$) for optimizing the ion optics for velocity map imaging depends somewhat on the z position of the REMPI laser. Thus the first step is to set z_{REMPI} to approximately the value that will be used in the experiments. Fortunately the dependence of R_{VMI} on z_{REMPI} is weak. From SIMION calculations performed with V_R set to 1500 V (the typical value used in our experiments) we find the optimum value V_E changes by only $\sim$14 V/mm, meaning an initial alignment within 1 mm of the nominal value of z_{REMPI} is sufficient. This accuracy is easily achieved, for example, by reference

to the center windows on the chamber or by referencing the position of the REMPI laser beam to the point where it scatters from the sample holder. We will show below that the laser beam can be set to the desired value of z_{REMPI} much more precisely.

To set V_R and V_E we used images from photolysis of gas phase CH_3Br. We can obtain Br and Br* signal easily by one photon photodissociation followed by 2+1 REMPI of Br or Br* ~ 234 nm. We first set V_R to 1500 V. We then adjusted the voltage on the extractor and found that $V_E = 1130$ V gave the sharpest VMI images with $z_{REMPI} \approx 1.5$ mm. Since V_R affects the magnification of the VMI optics, setting V_R to 1500 V was needed to keep the surface and gas phase images within the range of the multichannel plate/charge-coupled device camera imaging system as we are employing a rather long flight tube, 1050 mm. Using a shorter flight tube would result in possibly using smaller voltages.

For gas-phase VMI calibration, we used two methods to introduce CH_3Br. In our earlier work,[13] we introduced CH_3Br via an effusive beam along the z-axis of the apparatus. Here, we introduced CH_3Br as background gas at a pressure of $\sim 5 \times 10^{-7}$ Torr. The images taken with the effusive source were sharper than those from background gas, of course. Nonetheless we chose not to use the molecular beam in the present study as we feared moving the effusive beam source in and out of position might result in changes to the experimental conditions, for example, the electric fields, present in comparison to the surface desorption experiments. Despite these concerns, the results obtained with the "background gas approach" for obtaining the optimum value of V_E were in good agreement with those obtained with the effusive molecular beam.[13]

For future work, it could be desirable to find a way to introduce a molecular beam with the crystal in place. This might be accomplished, for example, by cutting a small hole in the center of the crystal and using this hole as the aperture for a molecular beam.

Photodissociation of gas phase CH_3Br at 234 nm gives Br atoms with a known velocity. We used this to establish the velocity calibration of the velocity map image. We found the calibration to be 8.4 pixel/m s^{-1}.

B. Parallelism of the surface and repeller plate

At first glance it might seem that the alignment of the surface relative the repeller plate would not be very critical. If we take θ_S to be the angle of the surface normal to the repeller plate normal, a misalignment by θ_S would add $v_z \sin(\theta)$ to v_x or v_y. For $\theta_S = 1°$, this would only be less than 2% of v_z. We found, however, that the effect of misalignments of the angle of the surface and sample mount relative to the repeller had a much larger effect and distorted the velocity images in a dramatic way, reflecting undoubtedly influences on the electric fields in the vicinity of the ionization region. This taught us that the effect of the misalignment is not only to launch the velocity at an angle θ_S to the axis of the VMI ion optics but also to alter the electric fields within the ion optics.
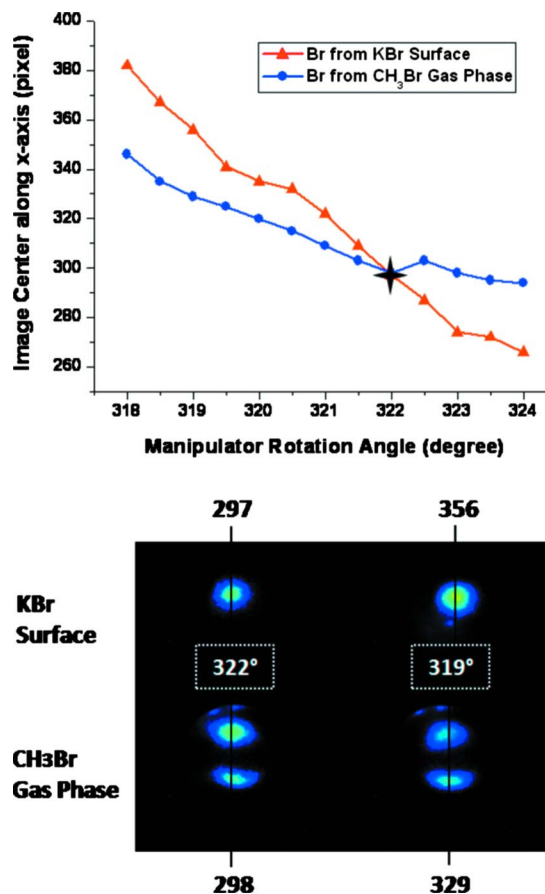

FIG. 3. (Color online) Image centers along the x-axis of Br from KBr surface photodesorption and Br from CH_3Br gas phase photodissociation and ionization. The figure shows the variation in the x-coordinate of the image centers as a function of the manipulator rotation angle; solid triangles represent Br from KBr surface photodesorption; solid circles Br from CH_3Br gas phase photodissociation. The star where the two curves cross is the optimized position for manipulator rotation stage. Two sets of images are also shown for illustration at the optimized position and nonoptimized position, respectively, in our measurement; the top images are for surface photodesorption and the bottom ones for CH_3Br photodissociation and photoionization. Images were taken with a manipulator rotation angle 322° for the optimized position and 319° for an example nonoptimized position.

To find the correct value of θ_S, we used a comparison of images of Br originating from surface photodesorption and Br originating from photoionization of CH_3Br background gas. We could rotate the crystal and sample holder about the y axis using the UHV sample manipulator. Unfortunately the manipulator did not have the ability to rotate about the x axis. We first took images of Br originating from photodesorption as a function of the rotation angle of the manipulator. We then introduced CH_3Br into the chamber as a background gas at a pressure of approximately 5×10^{-7} Torr and took images of Br from multiphoton ionization of this molecule at the same set of manipulator angles. We found the center position of each image by finding the center of gravity using BASEX image processing program.[19]

The results of how the x component of the centers of the images originating from gas phase and surface photochemistry move with the manipulator angle are plotted in Fig. 3. Note that as the manipulator angle is varied the center of
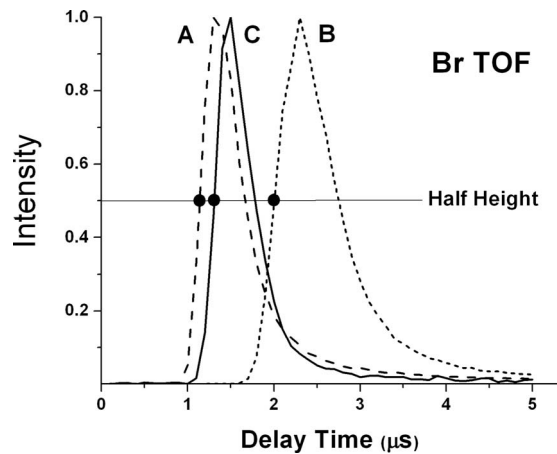
FIG. 4. Method for determining an accurate TOF distance. Curve A (dashed line) and curve B (dotted line) are measured using REMPI laser positions that differ by 1 mm. Curve C (solid line) is data recorded at the desired REMPI laser position, which is 1.5 mm away from KBr surface. Black circles mark the readings of the half-height point of each curve on the rising edge. See text for description of the calibration method.

both the gas phase and the surface velocity images change. The surface images, however, vary more strongly and there is a point where the curves cross and the surface and gas phase velocity map images have the same center point. This crossing gives the manipulator setting where the sample holder and repeller are parallel and hence the surface normal is directed along the TOF path.

C. Detection laser : Surface distance

For accurate absolute calibration of the velocities derived from our TOF measurements it is obviously necessary to know the distance, d, from the REMPI laser to the surface. We first established this distance approximately by finding a point where the laser beam hit the sample manipulator and then translating the laser beam 1.5 mm toward the ion detector. With this as a starting position we took a TOF curve—that is, by varying the delay between the desorption and detection laser pulses—of Br from laser photoexcitation of the KBr surface. Using micrometer driven translation stages on the mirror mounts used to steer the REMPI laser beam and focusing lens, we then increased z_{REMPI} by precisely 1.0 mm, nominally to 2.5 mm. The resulting TOF curves taken at the two flight distances are shown in Fig. 4. The curve at the earliest time (curve A) was recorded with the surface at its initial position, nominally 1.5 mm. The curve at the latest time (curve B) was recorded with the surface 1.0 mm further away. The intermediate curve (curve C) was recorded after the procedure we are about to describe.

We used the point at the half height on the leading edge of curves A and B to establish a velocity point that was common to the two curves. While one could choose other points along the TOF spectrum, the use of the half-height point gives us the best precision in the following procedure. We can then write $l_1 = vt_1$ and $l_2 = vt_2$, where v is the velocity corresponding the half-height point on the raising edge of the TOF curve, t_1 and t_2 are the corresponding times for curves

A and B, respectively, and l_1 and l_2 are the surface laser distances for curves A and B, respectively. Solving these equations we find

$$l_1 = t_1 \frac{(l_2 - l_1)}{(t_2 - t_1)}. \tag{2}$$

In the case shown in Fig. 2 we found $l_1 = 1.3$ mm. Since we wanted to work at a distance of 1.5 mm we used the micrometer driven stages to move the laser beam 0.2 mm further from the surface and recorded a TOF curve (curve C) at this distance. Note that curves A and C are easily distinguishable with a distance change of only 0.2 mm. We estimate the precision of this method in locating the desired flight distance is better than 0.05 mm. Note that the diffraction limited beam waist, $2\omega_0$, is 0.012 mm.

D. Position of the focal point in the *x-y* direction

The focus of the laser should be aligned in the x, y plane so it is on the symmetry axis of the VMI ion optics. This can be accomplished as follows. When operating in VMI mode, the optics effectively places the ionization point at the focal plane of the ion optics. In this configuration, parallel rays emitted anywhere from the ionization volume are focused on a point on the imaging detector. Choosing a different angle (which corresponds to a different transverse velocity) results in focusing to a different point on the detector. There is a 1:1 map between position on the detector and initial angle or velocity, hence the name "velocity map imaging."

It is also possible to operate the ion optics in a spatial imaging mode by changing the voltage on the extractor, V_E. By increasing V_E, we shorten the focal length of the ion optics. By choosing the focal length appropriately, we can then focus ions originating from a given spatial position to a point on the detector. This puts the optics into a spatial imaging mode. Using SIMION calculations and observations of the images, we found that a voltage of $V_E = 1500$ V, we obtained reasonably sharp spatial images as illustrated in Fig. 5. The images were recorded using Br originating from photo-desorption from the KBr surface. The images on the left were taken with $V_R = 1500$ V and $V_E = 1130$ V and are thus velocity map images. The images on the right were taken with $V_E = 1500$ V. The long bright region corresponds to an image of the laser beam. By using micrometer driven stages, we adjusted the y value until the center in VMI mode matched that found in spatial imaging mode. The images are quite sensitive to the ionization laser position. In our case, the image center moves at an average of 24 pixels per mm. We estimate that this method allows us to align the y value to within about 2 pixels or 0.08 mm. The same method can in principle be applied in the x direction. Here, however the method is less precise due to the lack of a sharp enough focus. Still we could easily align the position of the focus to better than 1.0 mm.

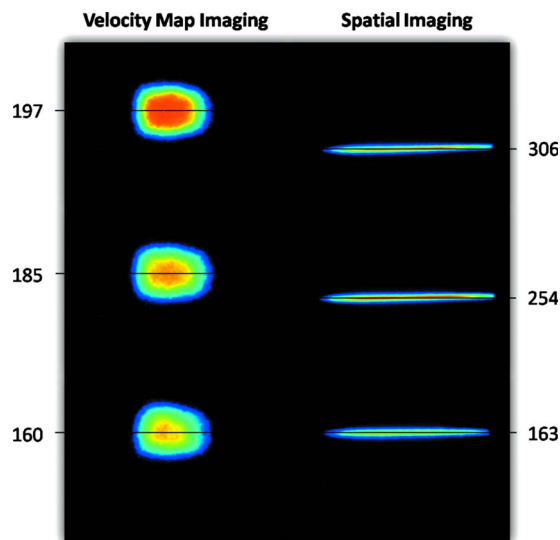**Velocity Map Imaging**   **Spatial Imaging**

FIG. 5. (Color online) Pairs of images taken in velocity map imaging mode (left) and spatial imaging mode (right) recorded at three different heights of the laser beam relative to the VMI ion optics a (*y*-axis position in Fig. 2). The *Y* coordinate (in pixels) of the center of the spatial and velocity map images are shown next to the respective images. The laser beam height at which the centers of the spatial and velocity map images line up represents the proper REMPI beam alignment.

IV. RESULTS AND DISCUSSION

We have found that TOF and image results obtained after performing the alignment procedures described are quite reproducible and the results generally agree with those reported previously.[13] There are some differences in the velocity images originating from the change in detection volume resulting from the use of a shorter focal length lens. We are currently collecting a systematic set of images and will present them in a subsequent publication.[20] Here we will concentrate on the TOF, velocity, and energy distributions of Br and Br* desorbed from the surface. Since we know that we have a good independent calibration of the distance between the surface and the ionization region, we can compare our results quantitatively to those obtained earlier.

TOF spectra for Br and Br* are shown in the upper panel of Fig. 6. These are transformed to velocity distributions in the middle panel, and energy distributions in the lower panel. Note that the TOF spectra, velocity distributions, and energy distributions refer to the motion of Br and Br* normal to the surface. The flux to density and Jacobian transformations used here are the same as we used previously.[13] The results for Br* clearly show a bimodal distributions. This indicates that the Br* desorption must involve at least two channels. For Br, although two peaks are not resolved, we also believe that two components contribute. We tried to fit the velocity distribution to a Gaussian as well as other functional forms, none of which were able to reproduce the data with a single contribution. A detailed discussion of this issue is beyond the scope of the present article and will be presented elsewhere.[20]

Multiple components in the velocity or energy distribution probably indicate multiple channels for the production of
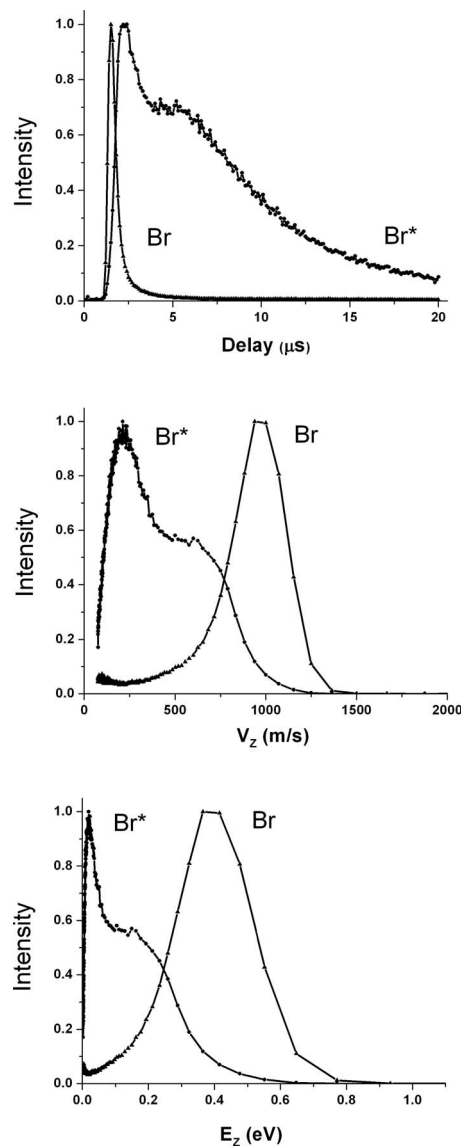

FIG. 6. TOF, velocity, and energy distributions for desorbing Br and Br*. Probability distributions for Br (open triangle) and Br* (open circle) desorbed from KBr surface. Top panel: TOF spectra. Middle panel: flux distribution as a function of v_z, the velocity component normal to the surface. Lower panel: flux distribution as a function of E_z, the energy associated with motion normal to the surface.

desorbing Br and Br*. For Br* the velocity distribution for the slow channel is slightly faster than that expected for thermal desorption at the surface temperature. The fast channel is clearly hyperthermal. It is interesting to speculate on possible mechanisms for multiple channels. They might originate, for example, from multiple desorption sites, such as steps or kinks versus terrace sites. It is also possible that one channel results from true surface desorption and the second comes from subsurface desorption. In the process of moving from the subsurface to the surface, the desorbing species could lose energy by collisions with surface atoms. For Br*, thermal desorption may also contribute to the slow peak. Other mechanisms might also play a role. We hope that a careful

examination of the velocity images in the *x*-*y* directions that come from the different components in the v_z distributions will help to elucidate the mechanism.

The present result are quantitatively more accurate but qualitatively similar to our previous result.[13] As before, we find two contributions to the TOF curve for both Br and Br*. For Br* the distributions are obviously bimodal, while for Br, we only see the contributions of multiple components by fitting. The velocity calibration is a little different in this set of results than in the previous set. Here, for example, we find the Br peak is at about 1000 m/s while in the earlier result we found the peak to be about 1200 m/s. This difference corresponds to a TOF distance error of $\sim$0.25 mm in the previous work, which is easily imaginable given our previous alignment procedures.

It is also interesting to compare these results to those obtained by Hess *et al.*[14] In contrast to our results, those experiments did not show bimodal or multiple component velocity or energy distributions from desorption with 193 nm (6.4 eV) photons. At present we cannot explain the reason for the difference but it may be related to differences in the angular acceptance of the detectors used in the two experiments or to other aspects of the setup. It is also possible that the differences relate to different crystals preparation techniques or different density of defects and steps. The actual energies reported in the two experiments are similar. Hess *et al.*[14] reported energies of approximately 0.34 and 0.20 eV at the peaks of the Br and Br* desorption distribution, respectively. This is to be compared to the present measurements of 0.39 eV for Br and 0.17 eV for the fast component of the Br*.

In summary, we have demonstrated a systematic alignment procedure for surface three-dimensional velocity map imaging. The alignment procedure uses observations of signals under actual operating conditions and thus is immune to changes in alignment that might occur for mundane reasons on a day to day basis. The procedure can be applied immediately before and after critical measurements to ensure that the alignment is correct initially and maintained during the course of the experiment. Under properly aligned conditions we have repeated the measurement of velocity distributions

in the normal direction to the surface. The results show small differences from our previous results that can be understood in terms of the differences in alignment that is within the expected error range of the previous alignment methods.

ACKNOWLEDGMENTS

[1] R. D. Levine and R. B. Bernstein, *Molecular Reaction Dynamics and Chemical Reactivity* (Oxford University Press, New York, 1987), pp. 67–116 and 207–502.

[2] R. I. Masel, *Principles of Adsorption and Reaction on Solid Surfaces* (Wiley, New York, 1996), pp. 354–437.

[3] C. T. Rettner, D. J. Auerbach, J. C. Tully, and A. W. Kleyn, J. Phys. Chem. **100**, 13021 (1996).

[4] D. J. Auerbach, in *Atomic and Molecular Beam Methods*, edited by G. Scoles (Oxford University Press, New York, 1988), Vol. 1.

[5] D. W. Chandler and P. L. Houston, J. Chem. Phys. **87**, 1445 (1987).

[6] A. T. J. B. Eppink and D. H. Parker, Rev. Sci. Instrum. **68**, 3477 (1997).

[7] M. N. R. Ashfold *et al.*, Phys. Chem. Chem. Phys. **8**, 26 (2006).

[8] T. J. Chuang, R. Schwarzwald, and A. Modl, J. Vac. Sci. Technol. A **9**, 1719 (1991).

[9] D. Corr and D. C. Jacobs, Rev. Sci. Instrum. **63**, 1969 (1992).

[10] P. H. Kobrin, G. A. Schick, J. P. Baxter, and N. Winograd, Rev. Sci. Instrum. **57**, 1354 (1986).

[11] M. Menges, B. Baumeister, K. Al-Shamery, H.-J. Freund, C. Fisher, and P. Andresen, Surf. Sci. **316**, 103 (1994).

[12] R. Schwarzwald, A. Modl, and T. J. Chuang, Surf. Sci. **242**, 437 (1991).

[13] S. P. K. Koehler, Y. Y. Ji, D. J. Auerbach, and A. M. Wodtke, Phys. Chem. Chem. Phys. **11**, 7540 (2009).

[14] W. P. Hess, A. G. Joly, D. P. Gerrity, K. M. Beck, P. V. Sushko, and A. L. Shluger, J. Chem. Phys. **115**, 9463 (2001).

[15] W. P. Hess, A. G. Joly, K. M. Beck, P. V. Sushko, and A. L. Shluger, Surf. Sci. **564**, 62 (2004).

[16] A. Eppink and D. H. Parker, J. Chem. Phys. **110**, 832 (1999).

[17] D. H. Parker and A. Eppink, J. Chem. Phys. **107**, 2357 (1997).

[18] D. A. Chestakov, S.-M. Wu, G. Wu, D. H. Parker, A. T. J. B. Eppink, and T. N. Kitsopoulos, J. Phys. Chem. A **108**, 8100 (2004).

[19] V. Dribinski, A. Ossadtchi, V. A. Mandelshtam, and H. Reisler, Rev. Sci. Instrum. **73**, 2634 (2002).

[20] Y. Ji, S. P. K. Koehler, D. J. Auerbach, and A. M. Wodtke (in preparation).